Crystallizing Sub 10 nm Covalent Organic Framework Thin Films via Interfacial-Residual Concomitance

Ashok Kumar Mahato,[1,2†] Saikat Bag,[1,2†] Himadri Sekhar Sasmal,[1,2*] Kaushik Dey,[1,2] Indrajit Giri,[1,2] Mercedes Linares-Moreau,[3] Carlos Carbonell,[3] Paolo Falcaro,[3*] E. Bhoje Gowd,[4,5] Ratheesh K Vijayaraghavan[1,2*] and Rahul Banerjee[1,2*]

[1]Department of Chemical Sciences, Indian Institute of Science Education and Research, Kolkata, Mohanpur 741246, India.

[2]Centre for Advanced Functional Materials, Indian Institute of Science Education and Research, Kolkata, Mohanpur 741246, India.

[3]Institute of Physical and Theoretical Chemistry, Graz University of Technology, Graz 8010, Austria.

[4]Materials Science and Technology Division, CSIR-National Institute for Interdisciplinary Science and Technology, Trivandrum 695019, Kerala, India.

[5]Academy of Scientific and Innovative Research (AcSIR), Ghaziabad 201 002, India.

*Email: himadrisasmal4@gmail.com; Tel: +033-6136-0000-1512

*Email: paolo.falcaro@tugraz.at; Tel: +43 316 873 32203.

*Email: ratheesh@iiserkol.ac.in; Tel: +033-6136-0000-1305.

*Email: r.banerjee@iiserkol.ac.in; Tel: +033-6136-0000-1327.

ABSTRACT: Synthesis of covalent organic framework (COF) thin films on different supports with high crystallinity and porosity is crucial for their potential applications. We have designed a new synchronized methodology, Residual Crystallization (RC), to synthesize sub 10 nm COF thin films. These residual crystallized COF thin films showcase high surface area, crystallinity, and conductivity at room temperature. We have used interfacial crystallization (IC) as a rate-controlling tool for simultaneous residual crystallization. We have also diversified the methodology of residual crystallization by utilizing two different crystallization pathways: fiber-to-film (**F–F**) and sphere-to-film (**S–F**). In both cases, we could obtain continuous COF thin films with high crystallinity and porosity grown on various substrates (the highest surface area of TpAzo COF thin film being 2093 m^2g^{-1}). Precise control over the crystallization allows the synthesis of macroscopic defect-free sub 10 nm COF thin films with a minimum thickness of ~1.8 nm. We have synthesized two COF thin films (TpAzo and TpDPP) using fiber-to-film (**F–F**) and sphere-to-film (**S–F**) pathways on different supports like borosilicate glass, FTO, silicon, Cu, metal and ITO. Also, we have investigated the mechanism of the growth of these thin films on various substrates with different wettability. Further, hydrophilic support (glass) was used to grow the thin films in-situ for four-probe system device fabrication. All residual crystallized COF thin films exhibit outstanding conductivity values. We could obtain a conductivity of 0.037 $mScm^{-1}$ for the TpAzo film synthesized by **F-F** residual crystallization.

INTRODUCTION

The degree of crystallinity and the orderliness of the crystallites within the bulk entity eminently control the physico-chemical properties of crystalline polymers.[1] However, gaining control over the crystallization of covalently linked polymeric structures with long-range order, i.e., covalent organic frameworks (COFs), is challenging.[2] The control over the self-assembly of the crystallites is of paramount importance in fabricating such crystalline COFs with the desired morphology.[3] In recent years, efforts have been directed towards manufacturing COF thin films, a morphology with immense potential for applications requiring a fast charge and mass transport.[4] In particular, large-area films with ordered pore channels and oriented crystalline domains are ideal for nano-filtration, electronic devices, and electrocatalysis.[5] COF thin films have been synthesized either *via* growing on support or using interfacial crystallization (IC).[6] The support assisted growth method produces small area crystalline films, which are challenging to scale up and lack generality across the COF framework composition. In interfacial crystallization, the monomers are dissolved separately in two immiscible solvents.[7, 8] The COF films developed in the liquid-liquid interface can easily be transferred to various substrates for several applications.[9,6a] However, the mobility of monomers at the liquid-liquid interface is not

uniform in the presence of two different phases, and only small domain sizes (generally tens of nanometers) have been obtained.[10] As a result, the thickness control requires optimization, and inhomogeneous films with non-uniform thicknesses, modest porosity, and crystallinity are often obtained. These undesired features drastically diminish the intrinsic conductivity and, films obtained by this method are often unsuitable for their electronic applications. In nanoelectronics devices, a bottom-up layer deposition would be an integrated approach for the active layer. Moreover, as the interfacial layer, sub 10 nm layers with high uniformity and defect-free topology would be essential to minimize the interfacial defects and facilitate the charge transfer processes. Hence, growing COF thin films directly on various solid substrates has been preferred for electronic device fabrication.[11, 6a, 6b]

Here, we report a unique synchronized protocol to synthesize highly oriented crystalline, porous, continuous COF thin films with uniform thickness on various substrates. We envisaged that precise spatial and temporal control over crystallization would be necessary for achieving such technologically relevant features. Hence, we have used a "*competing growth mechanism*" to prepare uniform thin COF layers on different solid substrates. This unique competing growth, where the bulk of the crystallization happens at the liquid-liquid interface and only the residues crystallize at the solid-liquid interface, has been termed "Residual Crystallization (RC)". COF thin films are grown on a device-relevant substrate using the residual crystallization approach with a 5-12 nanometers average roughness. The film thickness on the solid support is controlled by the rate of the interfacial crystallization at the liquid-liquid interface and ranges from 1.8 to 145 nm. This is the first report where the implementation of two parallel crystallizations within the same chemical reaction environment has been scheduled to steer the crystallization and self-assembly of the COF crystallites. The hydrophilicity of the solid substrates facilitates the crystallization, deriving thin films with an excellent degree of crystallinity and the highest surface area (2093 m^2g^{-1}) among the COF thin films reported to date. The superlative film growth on borosilicate glass with superior adhesion and negligible roughness provides an excellent conductivity of 0.037 $mScm^{-1}$.

RESULTS AND DISCUSSION

Two parallel interfaces, i) liquid-liquid and ii) solid-liquid within the same closed system, were created using a biphasic mixture consisting of two immiscible liquids [dichloromethane and water] (Figure 1a). The addition of reagents in two different phases helps to elude the direct mixing of the organic linkers and guide the simultaneous reaction-driven crystallizations at various interfaces. Two distinct residual crystallization methodologies have been coupled with the respective interfacial crystallization to acquire COF thin films. In the first case, the nanofiber-mediated interfacial crystallization has been brought into play. Whereas, in the second instance, nanosphere-mediated interfacial crystallization has been employed to induce residual crystallization. Hence, these methodologies are designated as i) fibers-to-film (**F–F**) and ii) spheres-to-film (**S–F**) methods. In the case of the **F–F** method, 0.075 mmol 1,3,5-triformylphloroglucinol (15.7 mg) are taken in 100 mL dichloromethane. Afterward, 0.112 mmol diamine linkers [4,4'-azodianiline (Azo, 23.7 mg); 3,8-diamino-6-phenylphenanthridine (DPP, 31.9 mg)] along with 0.58 mmol of *p*-toluenesulfonic acid (PTSA, 100 mg), dissolved in 50 mL of water is added dropwise on top of the organic solvent phase for synthesizing TpAzo and TpDPP COF thin films at the solid-liquid interface *via* residual crystallization (Figures 1c, 1e and S1). The organic diamine linkers slowly diffuse from the water phase to the organic phase through the liquid-liquid interface. The diffused diamine molecules react with the trialdehyde linkers in the organic phase *via* a dynamic covalent bond formation reaction. This process leads to COF crystallization at the solid-liquid interface to form one-dimensional (1D) COF fibers. The COF fibers further endure supramolecular interaction to generate 2D COF thin films.[12] A parallel interfacial crystallization of TpAzo and TpDPP COF thin films occurs in the liquid-liquid interface. The formation of TpAzo and TpDPP COF thin films at the liquid-liquid interface in parallel governs the diffusion and concentration of the primary building blocks in the organic phase. The liquid-liquid interface at the top slows down the amine diffusion and consequently the reaction rate, allowing slower crystallization and the growth of larger COF crystallites on the solid support at the bottom. Removing this interface barrier allows the direct mixing of amine and aldehyde molecules, leading to uneven and intermittent film growth (Figures 1b, S9, S13, S44a, and Section S-2).

In the second method (**S–F**), 100 mL of the as-synthesized COF nanosphere solution[3b, 12] (containing 3.5 mg of COF nanospheres) in dichloromethane is employed (Figures S1, S5-6, S11, S17, and S20). The liquid-liquid interfacial crystallization is introduced to integrate with the residual crystallization by dropwise addition of 100 mL deionized water on top of the COF nanosphere solution in dichloromethane. Consequently, most COF nanospheres present in the organic phase accumulate at the liquid-liquid interface. A few residual COF nanospheres slowly crystallize at the solid-liquid interface to generate COF thin film *via* residual crystallization (Figures 1d and S1). The absence of interfacial crystallization leads to uneven deposition of the COF nanospheres providing inhomogeneous, non-uniform COF films (Figures 1b, S9, S13, S44b, and Section S-2). It is noteworthy that TpAzo and TpDPP thin films grown on solid substrates could be separated from the surface directly by acid (1M H_2SO_4) treatment [13] (Figure S2). The variation of reagent concentration and reaction times allowed us to synthesize COF films of sub 10 nm thickness: $TpAzo_{F-F}$ ~1.8 nm (Ra ~0.8 nm), $TpDPP_{F-F}$ ~8.0 nm (Ra ~4.5 nm), $TpAzo_{S-F}$ ~6.1 nm (Ra ~2.3 nm) and $TpDPP_{S-F}$ ~8.0 nm (Ra ~3.6 nm) (Figure 1f-i). We placed the solid substrates at a vertically elevated position from the bottom end to investigate the crystallite growth at the solid-liquid interface. We find the uniform COF film formation at the top and bottom surfaces of the elevated solid substrate (Figures 1a, 2i-l, and

S18). The growth of COF thin films at the bottom surface of the substrate confirms that the thin films at the solid-liquid interfaces are not formed due to the gravity-induced sedimentation of crystallites. Instead, this thin film formation is due to the surface-induced assembly of crystallites, indicating the solid surface's role in crystallization.

The characteristic stretching frequencies in the Fourier transform infrared (FTIR) spectra at 1604–1623 cm^{-1} (–C=O), 1565–1576 cm^{-1} (–C=C), and 1232–1292 cm^{-1} (–C–N) indicates the formation of the β-keto-enamine backbone in all the synthesized COF thin films (interfacial and residual). Identical FTIR spectra of the COF thin films (TpAzo and TpDPP) in both the methodologies (**F–F** and **S–F**) reinforced the formation of the framework structures with similar chemical functionalities. Additionally, the absence of any amine –N–H stretching band at 3100–3400 cm^{-1} and aldehyde –C=O stretching band at 1636 cm^{-1} indicates the absence of free aldehyde and amine groups in the synthesized COF thin films (Figure S4-5). The powder X-ray diffraction (PXRD) patterns

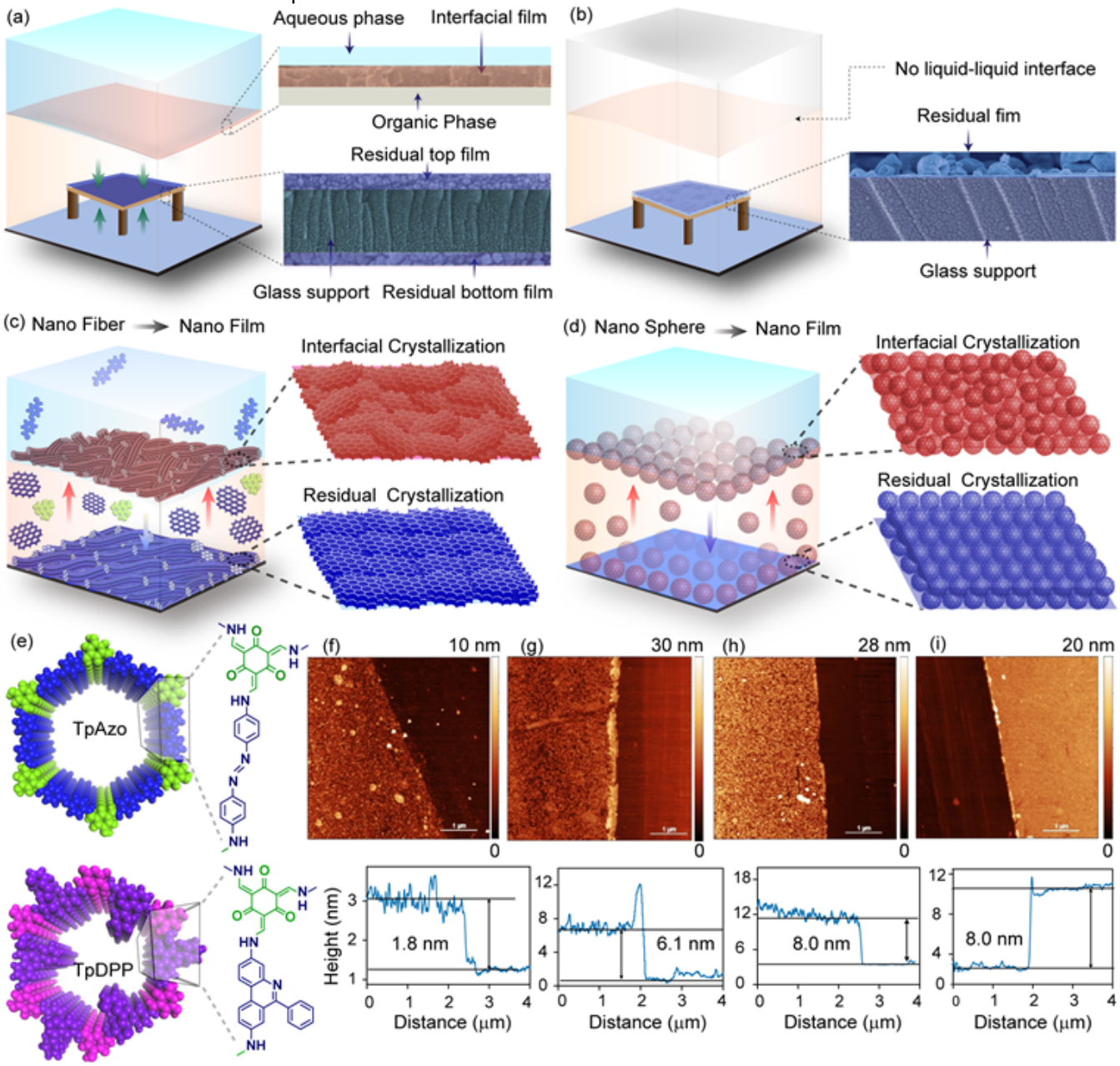

Figure 1. (a) Schematic representation of COF thin film fabrication at liquid-liquid and solid-liquid interfaces *via* interfacial and residual crystallization. The zoomed images represent the interfacial and residual (top and bottom surface of the substrate) COF thin films. (b) Residual crystallization in the absence of liquid-liquid interfacial crystallization. (c) Interfacial and residual crystallization processes *via* self-assembly of COF nanofibers. (d) Interfacial and residual processes *via* self-assembly of COF nanospheres. (e) Simulated eclipsed (AA) and slipped eclipsed (AA) structures of TpAzo and TpDPP COFs, respectively, with their chemical functionality. (f-i) AFM images of $TpAzo_{F-F}$, $TpAzo_{S-F}$, $TpDPP_{F-F}$, and $TpDPP_{S-F}$ thin films, respectively.

indicate the differences in the crystallinity of the interfacial and residual COF thin films. TpAzo and TpDPP COF thin films generate intense peaks at 2θ values 3.2±0.2° and 3.5±0.2°, respectively, which correspond to the diffraction from the (100) planes. The broad peaks at 2θ ~26–27° for $TpAzo_{F-F}$, $TpAzo_{S-F}$, $TpDPP_{F-F}$ and $TpDPP_{S-F}$ thin films are attributed to the diffraction from (001) planes indicating the π–π stacking (Figures 2a-d, S7, and S8). The distinguishable differences in the PXRD peak intensities of the (100) planes invigorated further investigation on their grain boundaries and defects. To investigate the differences in the crystalline domains, we have calculated the full width at half-maximum (fwhm) values of the peaks due to diffraction from the (100) planes of all residual and interfacial COF thin films. The fwhm values for the interfacial COF films are 0.449° ($TpAzo_{F-F}$) and 0.413° ($TpAzo_{S-F}$). In contrast, for residual crystallized COF thin films, the fwhm values are 0.361° ($TpAzo_{F-F}$) and 0.382° ($TpAzo_{S-F}$). Quite interestingly, the COF films crystallized by the residual crystallization on solid substrates showcase the most extensive crystalline domains among all these synthesized COF thin films. Raman spectroscopic data of all the sub 10 nm COF thin films further support the formation of the β-keto-enamine backbone (Figure S53-S54). For the TpAzo thin films ($TpAzo_{F-F}$ and $TpAzo_{S-}$

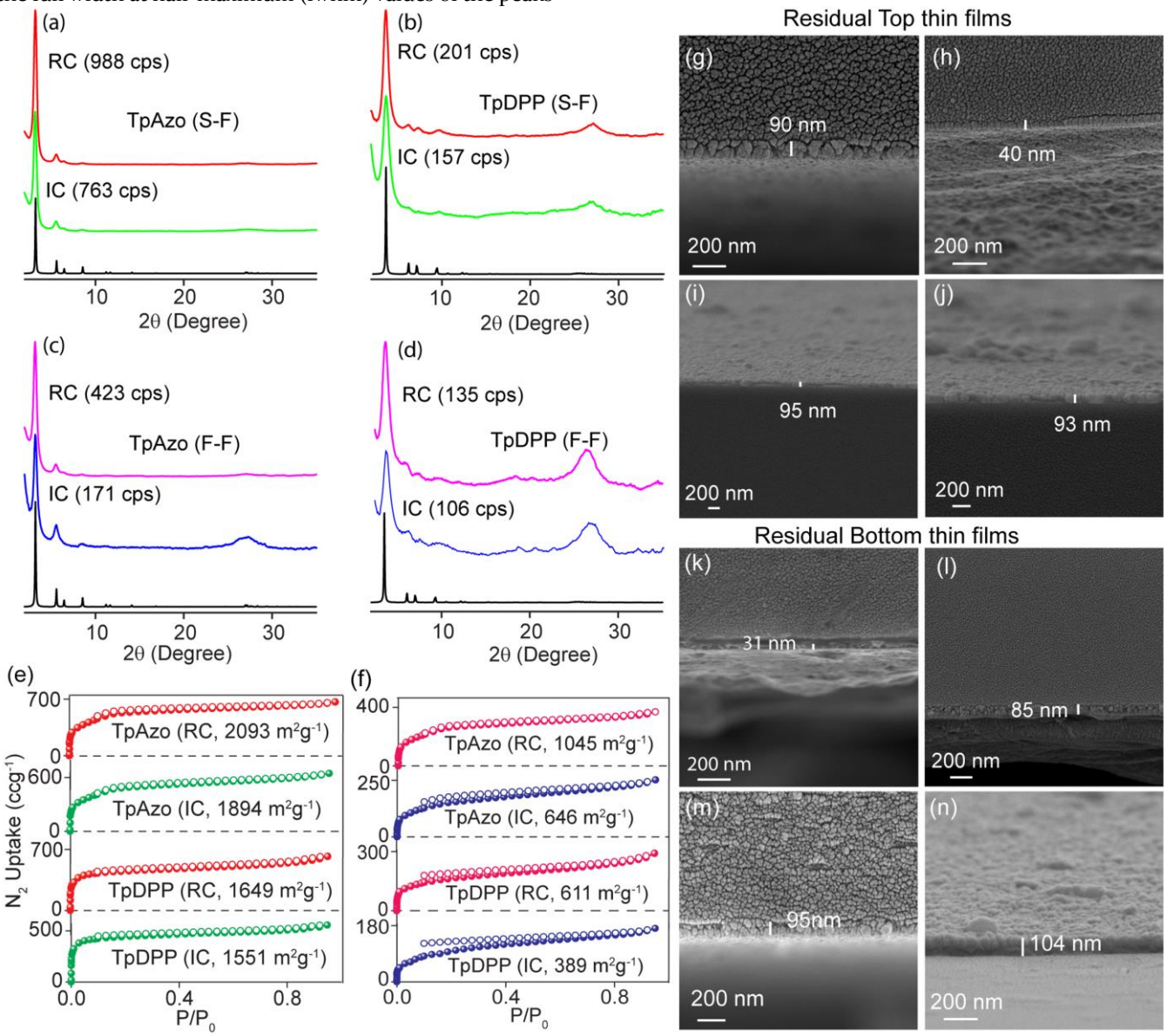

Figure 2. Powder X-ray diffraction (PXRD) patterns of residual (RC) and interfacial (IC) COF thin films synthesized by (a-b) **S–F** and (c-d) **F–F** methods. N_2 adsorption isotherm of TpAzo and TpDPP residual and interfacial COF thin films by (e) **S–F** and (f) **F–F** methodology. Cross-sectional SEM images of the $TpAzo_{F-F}$ (g), $TpDPP_{F-F}$ (h), $TpAzo_{S-F}$ (i)and $TpDPP_{S-F}$ (j) residual top films. Cross-sectional SEM images of the $TpAzo_{F-F}$ (k), $TpDPP_{F-F}$ (l), $TpAzo_{S-F}$ (m) and $TpDPP_{S-F}$ (n) residual bottom films.

$_F$), characteristic Raman peaks appear at 1600 cm^{-1} (C=C); 1450 and 1409 cm^{-1} (N=N); 1139 cm^{-1} (C–N), whereas the TpDPP films show the peaks at 1613 (C=C) and 1357-1416 cm^{-1} (phenanthridine moiety).[14] The Brunauer–Emmett–Teller (BET) surface areas of the COF thin films (using borosilicate glass as the solid substrate) have obtained in the **S–F** method are calculated as 2093 ($TpAzo_{S-F}$) and 1649 ($TpDPP_{S-F}$) m^2g^{-1}. The COF thin films synthesized *via* the **F–F** method exhibit comparably less BET surface areas of 1045 ($TpAzo_{F-F}$) and 611 m^2g^{-1} ($TpDPP_{F-F}$) (Figures 2e-f, S12, and S14). The parallel process of interfacial crystallization yields COF thin films at the liquid-liquid interface with surface area 1894 ($TpAzo_{S-F}$), 1551 ($TpDPP_{S-F}$), 646 ($TpAzo_{F-F}$), and 389 ($TpDPP_{F-F}$) m^2g^{-1}, respectively (Figures 2e-f, and S15). Thermogravimetric analysis (TGA) of COF thin films synthesized *via* residual and interfacial crystallization reveals their thermal stability up to 300 °C (Figure S21). This reinforces the fact that the chemical functionalities of the underlying structural backbone of the COF crystallites are identical despite their difference in crystallization. Cross-sectional scanning electron microscopy (SEM) images reveal the formation of the residual COF thin films with thickness between 40 to 104 nm (Figure 2g-n). The maximum thickness of the thin films ranges between 100-145 nm for all the residual COF films (Figure S18).

We have utilized UV-vis spectroscopy and dynamic light scattering (DLS) analysis to grasp the mechanistic insight of the residual crystallization process. The UV-vis spectroscopic data reveals two simultaneous processes during the crystallization in the **F-F** method. The first process concerns the diffusion by which the Azo amine molecules in water diffuse into the dichloromethane layer through the water-dichloromethane interface. The Azo amine in water exhibits an absorption maximum at 390 nm. The absorbance of these Azo amine molecules in the aqueous solution decreases with

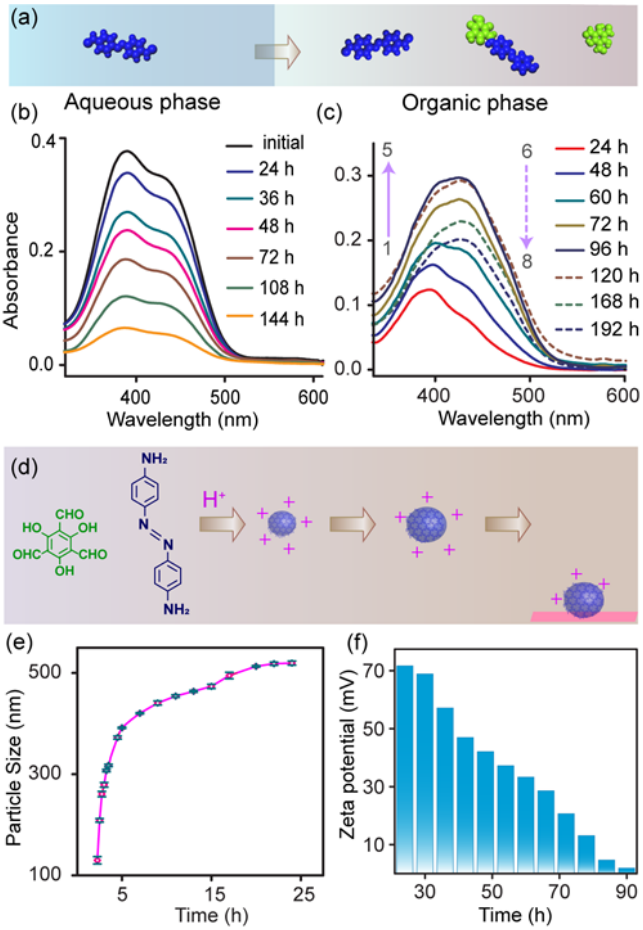

Figure 3. (a) Diffusion of amine in **F-F** method (b-c) UV-vis absorption spectrum of Azo amine with the progress of the reaction in both the water and dichloromethane layer, respectively. (d) Schematic of the synthesis of COF nanospheres and subsequent crystallization. (e) Time-dependent particle size measurement of TpAzo COF nanospheres. (f) Zeta potential measurement over time with the progress of the reaction.

time because of their diffusion into the organic phase (Figures 3a, 3b, and S22a). The Azo amine concentration in water reduces gradually with an initial absorbance of 0.377 to 0.047 after 144 h. Consequently, the Azo amine concentration in dichloromethane increases slowly from the absorbance of 0.09 (after 12 h) to 0.297 after 96 h. In the second process, this diffused Azo amine molecules in the dichloromethane layer initiate the reversible Schiff base reaction with aldehyde linkers to produce the oligomers (Figure S24). As the reaction progresses, the aldehyde concentration present in the dichloromethane layer (maximum absorption band at 267 nm) linearly decreases (absorbance ~0.889 to 0.445 after 192 h) while reacting with the amine to produce oligomers (Figure S22c). The evolved oligomers instigate the reaction-driven crystallization at the solid-liquid interface. After 96 h, the diffusion of the Azo amine from the aqueous phase to the organic phase subsides, and the oligomer formation process becomes predominant over the diffusion. Consequently, amine concentration in the

organic phase starts to decrease, and the elevated absorbance of 0.297 (after 96 h of reaction) reduces to 0.201 after 192 h (Figures 3c and S22b).

The crystallization and the dynamic self-assembly of the COF crystallites are crucial in reducing the grain boundaries and defects within the thin films. In the event of **S–F** residual crystallization, time-dependent DLS analysis of the reaction mixture reveals the formation of COF nanospheres having an average size of 390 nm (TpAzo) and 279 nm (TpDPP) after 5 h of refluxing. These COF nanospheres slowly grow to 529 nm (TpAzo) and 453 nm (TpDPP) upon reacting with free aldehydes and amines in the solution and finally, after 24 h form a colloidal solution (Figures 3d, 3e, and S25). Time-dependent UV-vis spectra confirm the continuous consumption of the aldehyde and amine molecules during the synthesis of COF nanospheres. The initial absorbances of aldehyde (0.81) and amine (0.46) are reduced to 0.19 and 0.17, respectively, after 24 h of refluxing (Figures 3d and S23). The zeta potentials of as-synthesized $TpAzo_{S-F}$ and $TpDPP_{S-F}$ COF nanosphere are 71.7 and 77.6 mV respectively at 20°C, which indicates the stable positive charges (mainly due to the protonated free $-NH_3^+$ groups on their surface). When water is added dropwise on top of the colloidal COF nanospheres in dichloromethane, the COF nanospheres start assembling at the liquid-liquid and the solid-liquid interfaces. The zeta potential of the deposited COF nanosphere drops to 1.9 mV ($TpAzo_{S-F}$) and 0.6 mV ($TpDPP_{S-F}$) after 90 h (Figures 3f and S25). This distinctly indicates that when the COF nanospheres come in contact, the electrostatic repulsion and subsequent energy destabilization of the COF nano-spheres promote the disassembly. This electrostatic repulsion decreases as the zeta potential decreases with the progress of crystallization. The presence of free amine and aldehyde functionality in the COF nanospheres steers the dynamic self-assembly among the disassembled COF crystallites. Thus, transmuting them into the COF nanofibers and eventually materializing them as continuous and macroscopic defect-free COF thin films. Time-dependent FTIR analysis reveals the disappearance of free $-NH_3^+$ from the sphere surface, which discloses the decrease of positive zeta potential charges with the progress of reaction (Figure S31b).

Close inspection of the SEM and TEM images at different time intervals showcase the mechanistic pathways for the residual crystallization on the solid-liquid interface. We could isolate $TpAzo_{F-F}$ crystallites with an average dimension of ~5 nm after 24 h of reaction. As the reaction proceeds, $TpAzo_{F-F}$ crystallites start to grow larger (~10 nm) and assemble predominantly in one direction [longitudinal growth (~30–120 nm) > lateral growth (~5–15 nm)] to evolve as nanofibers. The lateral dimensions of the $TpAzo_{F-F}$ nanofibers increase up to ~50 nm, whereas the length of the fibers up to ~1 μm. The emerging $TpAzo_{F-F}$ nanofibers hold themselves together by H-bonding and other supramolecular interactions.[15] Their lateral connection gives rise to a sheet-like assembly with the average lateral dimension of ~2 μm after 60 h of reaction. After 96 h, almost all the $TpAzo_{F-F}$ nanofibers are converted into a uniform two-dimensional thin-film entirely covering the surface of the solid substrate (Figures 4a-k, S26, S47 and S49). Incidentally, we have observed an interesting morphological transformation from 0D nanospheres (~500 nm) →1D nanofibers (length ~350 nm and diameter ~40 nm) →2D thin films having a lateral dimension of 2-3 μm for the **S–F** method (Figures 4m-w, S48 and S50). During the residual crystallization, disassembly of the TpAzo COF nanospheres at the solid-liquid interface is visualized. This disassembly has been identified as the "bursting" of the COF nanospheres (~300-400 nm)

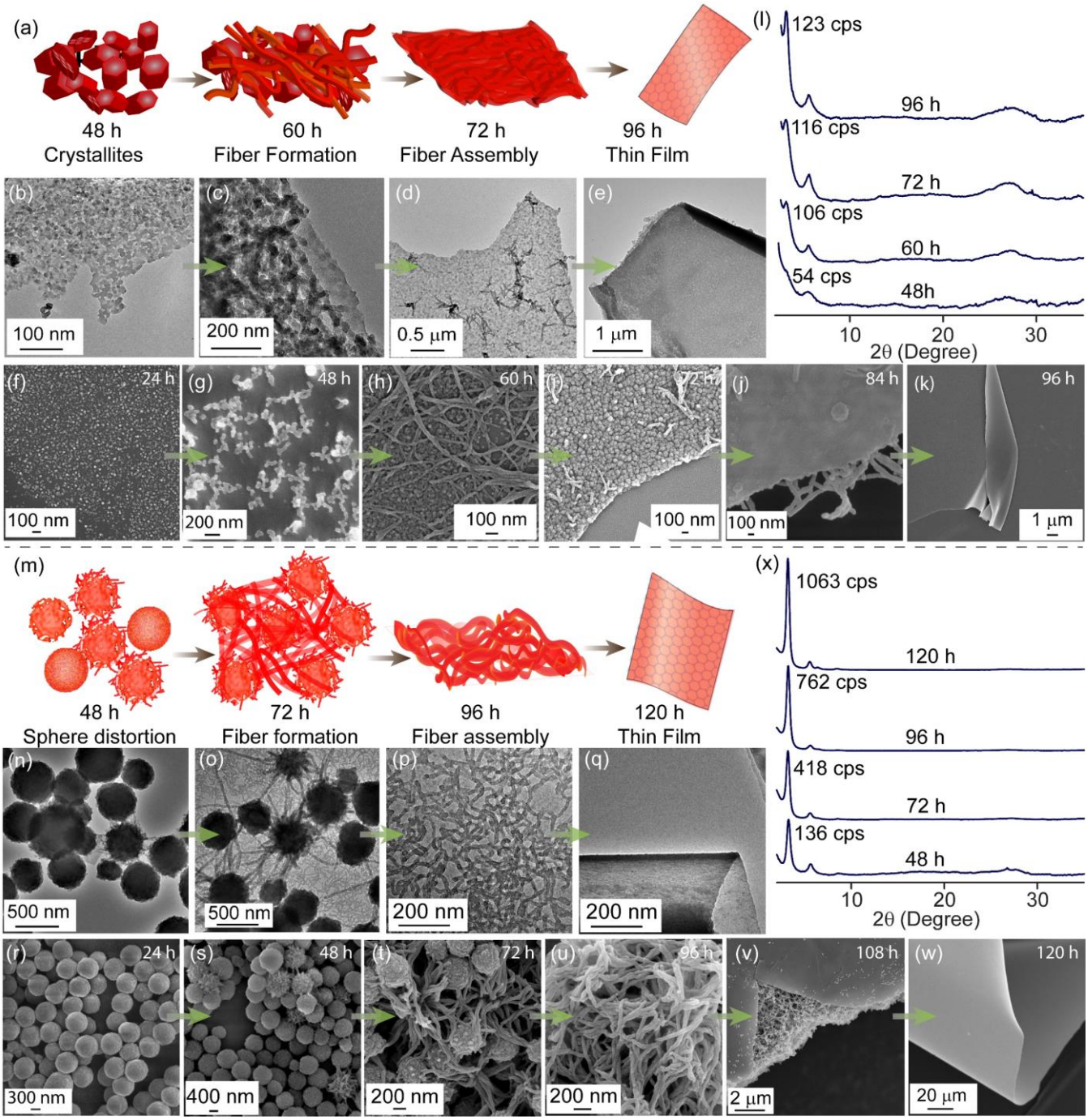

Figure 4. (a, m) Schematic of various stages during thin film synthesis by **F–F** and **S–F** methodology. (b-e) and (f-k) Time-dependent TEM and SEM images of different morphologies during thin film synthesis by **F–F** methodology. (n-q) and (r-w) Time-dependent TEM and SEM images of different morphologies during thin film synthesis by **S–F** methodology. (l, x) Time-dependent PXRD pattern at a different time interval during TpAzo COF thin film synthesis by (**F–F**) and (**S–F**), respectively.

into nano threads (~50-100 nm) projecting over the surface.[16] The reaction-driven disassembly triggers the other nanospheres in close proximity to ultimately transmute into crystalline threads (150-350 nm). These thread-like nano-crystallites are further interconnected and fused *via* dynamic covalent self-assembly to convert into COF thin films after 120 h (Figure S27-S30).

The time-dependent PXRD analyses provide a better understanding of the continuous crystallite growth throughout the residual crystallization process. In the case of **F–F** method, PXRD patterns obtained from the assembled particles at the solid-liquid interface after 48 h of reaction reveal the particles to be crystalline with the diffraction peak from (100) planes at 2θ = 3.2° (cps ~54) (Figures 4l and S52). The domain size of the COF

crystallites increases with time, which is reflected in their intensified diffraction peak of (100) planes (cps ~106). The COF crystallites rearrange with more order and periodicity after 70 h because of the π-π stacking and H-bonding driven self-assembly process. Crystallization and the assembly of the COF crystallites after 96 h, leads to the formation of COF thin films with high crystallinity (cps ~123). The rearrangement of the COF crystallites at the solid-liquid interface in the **S–F** method increases crystallinity (cps ~136) due to the initiation of dynamic covalent self-assembly (48 h) among TpAzo COF nanospheres. After 72 h, the COF crystallites start minimizing the grain boundaries and crystal defects (cps ~418) due to this covalent self-assembly (72 h) among the COF nanospheres (Figures 4x and S52). Completing the covalent self-assembly of the TpAzo COF crystallites leads to the formation of highly crystalline COF thin films (cps ~1063) after 120 h.

We have also observed the change in functionality associated with the crystallites (**F–F**) and the nanospheres (**S–F**), by time-dependent FTIR spectroscopy. The peaks for free $-NH_2$ and free –CHO groups [3383 and 3352 ($-NH_2$); 2926 and 2866 (–C–H); 1733 (–CH=O) cm^{-1}] are present after 48 h of reaction in the **F–F** method. After 72 h, we have observed the complete disappearance of the free $-NH_2$ and free –CHO peaks (Figures S31a and S51a). In the case of **S–F** method, initially (48 h), we observed the presence of free $-NH_2$ and free –CHO peaks [3345 and 3214 ($-NH_2$); 2917 and 2850 (–C(O)–H); 1719 (–CH=O) cm^{-1}] on the sphere surface. As the reaction proceeds, all the peaks of free $-NH_2$ and free –CHO start to disappear, and after 96 h, these peaks are completely dissipated (Figures S31b and S51b).

The applicability and the performance of the synthesized COF thin films in numerous applications such as electrochemical device fabrication or selective molecular separation, require precise controlled crystallization and large area uniform macroscopic defect-free growth of crystallites on solid substrates. Thus, we have investigated a wide range of substrates to realize the full potential of the residual crystallization. Solid supports with a wide range of wetting and adhesion interactions with water were employed to scrutinize residual crystallization's essential suitability aspects. We found that both the residual crystallization methodologies (**F-F** and **S-F**) rely on the nature (wettability) of the substrate surface. Residual crystallization also depends on the surface charge, chemical interaction between the crystallites, and substrate roughness. Hence, we used solid substrates with different wettability and adhesion towards water molecules to investigate the applicability of the residual crystallization. Borosilicate glass [(contact angle CA ~55.2°)], FTO (CA ~72.9°), silicon wafer (CA ~73.9°), metallic copper-plate (CA ~95.9°), ITO [(CA) ~97.7°], and polytetrafluoroethylene (CA ~102.6°) were exploited as the substrates with a wettability ranging from hydrophilic to hydrophobic (Figures 5a, S3, and S32). For all the solid substrates, the isolated COF thin films show characteristic PXRD patterns with the intense peak at 2θ = 3.2° (TpAz0) and 3.7° (TpDPP) corresponding to (100) plane and 2θ = 26-27° (both TpAz0 and TpDPP) corresponding to (001) plane of the underlying COF framework structures (Figure S33-34). The fwhm values were calculated from the diffraction peak of (100) planes. The films grown on hydrophilic support (CA < 90°) were found to be more crystalline compared to the thin films produced on hydrophobic support. The lower fwhm values (0.361-0.441° for TpAzo and 0.621-0.687° for TpDPP) of the thin films grown on hydrophilic substrates propounded for the larger crystallite size. In contradiction, higher fwhm values suggested a smaller crystallite size of the COF thin films grown on the hydrophobic surfaces (Figure 5c). Characteristic FTIR bands (1616-1597 for C=O, 1537-1576 for C=C, and 1229-1275 cm^{-1} for C–N stretching frequency) obtained from the COF thin films fabricated on different substrates indicate the formation of the β-ketoenamine backbone structure (Figures S37-38). TpAzo and TpDPP thin films precipitate as crystalline particles when we try to crystallize them on hydrophobic surfaces like polytetrafluoroethylene (CA ~102.6°). The surface areas of the COF thin films grown on hydrophilic surfaces (1590 – 2093 m^2g^{-1} for $TpAz0_{S-F}$, 791 – 1045 m^2g^{-1} for $TpAz0_{F-F}$, 1073 – 1649 m^2g^{-1} for $TpDPP_{S-F}$, and 274 – 611 m^2g^{-1} for $TpDPP_{F-F}$) are higher compared to the surface areas of the COF thin films grown on a hydrophobic supports [(CA ~95.9° to 97.7°) 930 – 1133 m^2g^{-1} for $TpAz0_{S-F}$, 312 – 745 m^2g^{-1} for $TpAz0_{F-F}$, 921 – 1006 m^2g^{-1} for $TpDPP_{S-F}$, and 142 – 258 m^2g^{-1} for $TpDPP_{F-F}$)] (Figures 5b and S35-36). SEM images of the films (**F–F** and **S–F**) reveal continuous film growth on the supports except on the very hydrophobic one (polytetrafluoroethylene) (Figures S39-43). The hydrophilicity of the substrates facilitates the crystallization and self-assembly of the COF crystallites, yielding thin films with an excellent degree of crystallinity and the highest surface area (2093 $m^2\ g^{-1}$) among the COF thin films reported to date (Table S1).

To understand the electrical conductivity of the 2D COF films, a well-known van der Pauw method has been followed, as described in detail below.[17] Various thin film parameters like the thickness and kinetics of the film growth to yield diverse film quality are analyzed. The surface roughness is kept as low as possible (Ra ~5-12 nm) to get the accurate thickness of the film. An optimum film thickness of 120±20 nm is used for all the cases to quash the effect of the film thickness on the measured conductance.[18] The samples are grown in-situ on cleaned glass substrates and then washed thoroughly using chloroform and ethanol solvents to remove any trapped impurities or reagents and are dried in a vacuum at room temperature for 24 h. Au electrodes (~300 nm) are deposited on the films defining a square geometry of the electrode structure (Figure S45a), ensured using appropriate shadow masks for electrode deposition. 18-20 devices of each substrate are prepared, and the I-V characteristics of each device are analyzed using a probe station coupled with a semiconductor parameter analyzer Keithley SCS 4200. For the electrical characterization, two probes defining one edge of a square on the film's surface are assigned for the current bias (terminal B and C, figure 5d). The other two probes at the

opposite edge measure voltage (terminal A and D). Two orthogonal resistances are measured likewise where $R_{BC} = V_{AD}/I_{BC}$ and $R_{AB} = V_{DC}/I_{AB}$. The electrical conductivity (σ) is calculated based on those two resistances and the thickness of the sample[19] using the following equation.

$$\sigma = \frac{ln2}{\pi t} \times \frac{2}{(R_{AB}+R_{BC})f(\frac{R_{AB}}{R_{BC}})}$$

Where t, is the film thickness and f is assigned to be 1.[20] I_{BC}-V_{AD} of films grown by residual methods, represented in figure 5f. The average conductivity of 20 devices with the standard deviation is represented in figure 5g. We synthesized the TpAzo COF films using residual crystallization and four other methods *viz*. interfacial crystallization (Figures 2a-d, 2g-h, S15, and S19), direct synthesis [Figures 5e (3), S9, S13, and Section S-2], solvothermal synthesis [Figures 5e (4), S10a, S16a, and Section S-2], and spin coating [Figures 5e (5), S10b, S16b and Section S-2]. We have performed the conductivity measurement with the films grown on a glass support. The 2-D conductivity of the films obtained by the residual

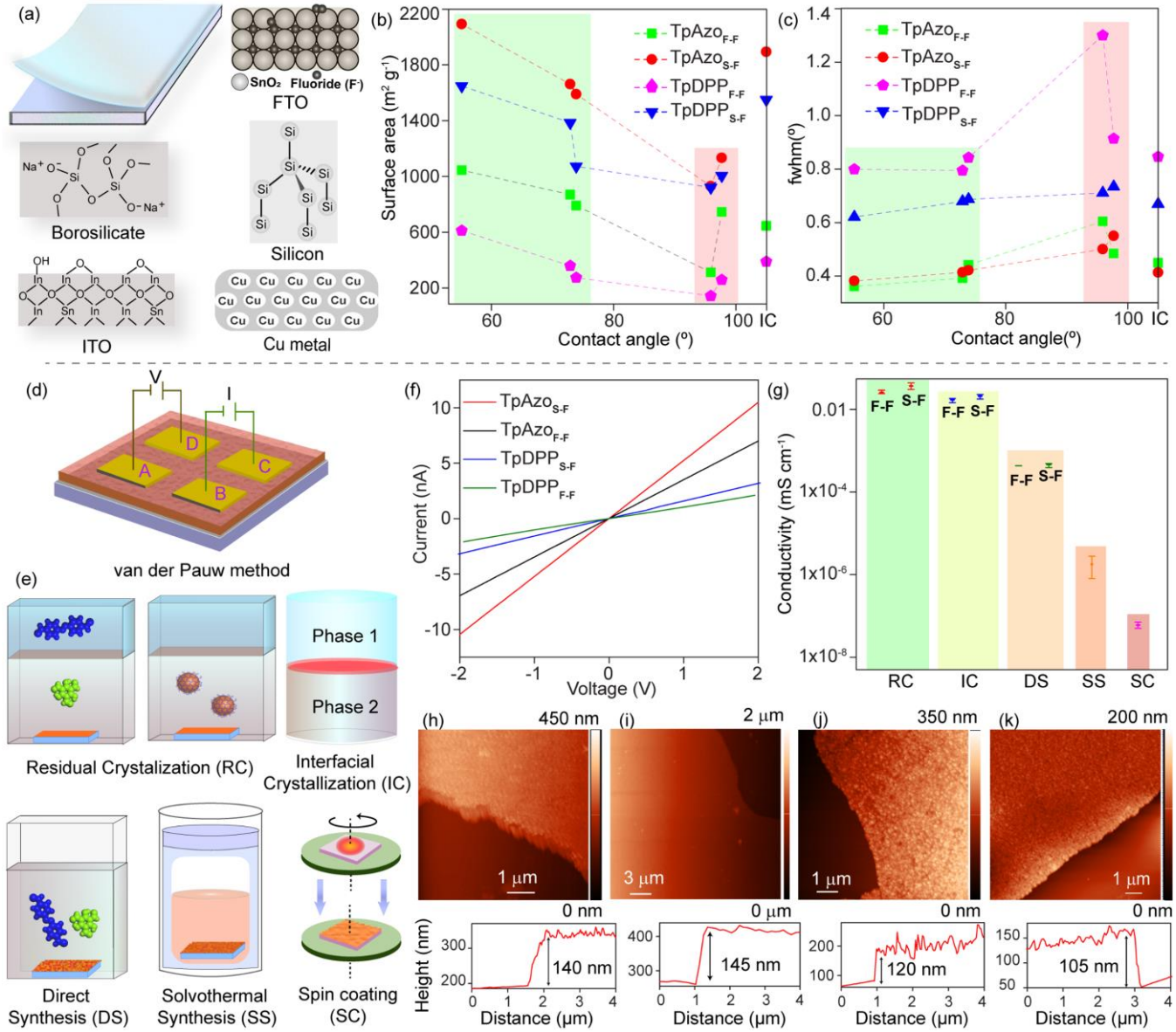

Figure 5. (a) Schematic of film grown on a support and the chemical structures of different supports (Borosilicate glass, ITO, FTO, Silicon wafer, and Copper metal). (b) Surface areas and (c) fwhm values of TpAzo and TpDPP films concerning different contact angles of different supports. (d) Schematic of four-probe system devices for conductivity measurement. (e) Various methodologies of thin-film fabrication. (f) I-V characteristics of the planar devices out of films of residual crystallization. (g) Conductivity data of the thin films obtained by different methods are shown in (e). (h-k) AFM images of the thin films fabricated by residual crystallization, with the corresponding height profiles.

crystallization method has outperformed the conductivity obtained for the other methods (Figure 5g). An average conductivity of 3.7 x.10^{-2} and 2.6 x10^{-2} mScm^{-1} are obtained for the films grown by **S–F** and **F–F** methods, respectively (Tables S2 and S3). These conductivity values are 52% higher than the interfacial **F–F** and 75% higher than the

interfacial **S–F** films. Films grown by other methods *viz*, solvothermal or spin coating present conductivities four orders of magnitude lower than the films grown by the residual crystallization method. The order of the 2-D electrical conductivity is $\sigma_{\mathbf{S}\text{–}\mathbf{F}(RC)} > \sigma_{\mathbf{F}\text{–}\mathbf{F}(RC)} > \sigma_{\mathbf{S}\text{–}\mathbf{F}(IC)} > \sigma_{\mathbf{F}\text{–}\mathbf{F}(IC)} > \sigma_{(direct)} > \sigma_{(solvothermal)} > \sigma_{(spin\ coating)}$. Average conductivity is in the order of 10^{-2} mScm^{-1} for the films grown by RC method, whereas it is in the order of 10^{-4}—10^{-6}, 10^{-7} for the films grown by the other techniques. We believe that continuous, smooth, and macroscopic defect-free film growth with a strong attachment to the substrate affords the best conductivity with residual crystallized thin films (Table S3). Though the nature of the charge transport and the mechanism of 2D electrical conductivity is under investigation, the preliminary results indicate a correlation between the planar electrical conductivity and the type of film growth process. As the chemical structures are comprised of interrupted/broken sp^2 carbon conjugation, the probable transport mechanism could be a thermally activated hopping mode (Figure S45b). A detailed mechanistic investigation of the charge transport is in progress. To summarize, the electrical conductance obtained agrees with the other results discussed hitherto.

CONCLUSION

In conclusion, we have designed a unique synchronized methodology to fabricate highly crystalline COF thin films on different solid substrates. We have coupled the liquid-liquid interfacial crystallization and solid-liquid residual crystallization. The utilization of one crystallization process to augment another simultaneous crystallization to accomplish such continuous, macroscopic defect-free, precisely oriented, crystalline, and porous thin films with smooth surfaces and uniform thickness is still elusive. We could synthesize uniform, continuous COF thin films with high crystallinity and surface area (2093 m^{2}g^{-1} for the TpAzo film on glass support), with minimal surface roughness. We were able to reduce the thickness to the sub-10 nm level (~1.8 nm for TpAzo film) by varying reaction time and reducing the concentration of the starting materials during crystallization. We have widened the solid substrates based on the wettability and observed superior film growth on hydrophilic surfaces (Borosilicate glass, FTO, and silicon wafer). Quality film growth providing good electrochemical contact by this residual crystallization enables remarkably high conductivity (0.037 mScm^{-1} for TpAzo$_{F\text{–}F}$) of the COF thin films. High-capacity conversion materials generally undergo considerable structural changes, which can cause mechanical instability across the length scales of individual electrodes and photodetectors. Hence, future research in this area will require understanding the compositional chemistry of interfacial layers and approaches that allow for defect-free coatings of various architectures with varying porosity. This extensive evaluation of the residual crystallization controlled by another parallel interfacial crystallization to synthesize COF thin films on various supports could become a productive way for maximum utilization in multiple applications towards perfection.

ASSOCIATED CONTENT

Supporting Information. Synthesis, crystallography, and characterization details are provided in the Supporting Information file. This material is available free of charge *via* the Internet at.
http://pubs.acs.org.

AUTHOR INFORMATION

Corresponding Author
* himadrisasmal4@gmail.com
* paolo.falcaro@tugraz.at
* ratheesh@iiserkol.ac.in
* r.banerjee@iiserkol.ac.in

Author Contributions
†A.K.M. and S.B. contributed equally to this work.

ORCID
Rahul Banerjee: 0000-0002-3547-4746
Ratheesh K Vijayaraghavan: 0000-0001-8952-8087
E. Bhoje Gowd: 0000-0002-2878-5845
Paolo Falcaro: 0000-0001-5935-0409
Carlos Carbonell: 0000-0003-0089-8626
Mercedes Linares-Moreau: 0000-0003-3027-6238
Indrajit Giri: 0000-0002-8538-2241
Kaushik Dey: 0000-0003-4889-8035
Himadri Sekhar Sasmal: 0000-0001-7355-8783
Saikat Bag: 0000-0002-0464-2276
Ashok Kumar Mahato: 0000-0001-9517-1598

Notes
The authors declare no competing financial interests.

ACKNOWLEDGMENT

AKM, SB acknowledges CSIR for Research fellowship. KD acknowledges DST-SERB, India, for a RA fellowship [CRG/2018/000314]. RB. acknowledges SwarnaJayanti Fellowship grant [DST/SJF/CSA-02/2016-2017], DST Mission Innovation [DST/TM/EWO/MI/CCUS/17 and DST/TMD(EWO)/IC5-2018/01(C)], DST SERB [CRG/2018/000314] for funding. M.L.-M., C.C.C., and P.F. acknowledge European Union's Horizon 2020 Program (FP/2104-2020)/ERC Grant Agreement no. 771834 POPCRYSTAL and Anton Paar. The authors acknowledge the use of the Somapp Lab, a core facility supported by the Austrian Federal Ministry of Education, Science and Research, TU Graz, UNI Graz, and Anton Paar GmbH. We acknowledge Mr. Amal Raj R B for helping in PXRD data collection.

REFERENCES

1. (a) Yaghi, O.M.; Keeffe, M.O.; Ockwig, N.W.; Chae, H.K.; Eddaoudi, M.; Kim, J. Reticular synthesis and the design of new materials. *Nature* **2003**, 423, 705-714. (b) Zhao, Y.; Guo, L.; Gandara, F.; Ma, Y.; Liu, Z.; Zhu, C.; Lyu, H.; Trickett, C. A.; Kapustin, E. A.; Terasaki, O.; Yaghi, O.M. A Synthetic Route for Crystals of Woven Structures, Uniform Nanocrystals, and Thin Films of Imine Covalent Organic Frameworks. *J. Am. Chem. Soc*. **2017**, 139, 13166-13172. (c)

Kandambeth, S.; Dey, K.; Banerjee, R. Covalent Organic Frameworks: Chemistry beyond the Structure. *J. Am. Chem. Soc*. **2019**, 141, 1807-1822. (d) Zhao, X.; Pachfule, P.; Li, S.; Langenhahn, T.; Ye, M.; Schlesiger, C.; Praetz, S.; Schmidt, J.; Thomas, A. Macro/Microporous Covalent Organic Frameworks for Efficient Electrocatalysis. *J. Am. Chem. Soc*. **2019**, 141, 6623–6630. (e) Ji, Z.; Li, T.; Yaghi, O. M. Sequencing of metals in multivariate metal-organic frameworks. *Science* **2020**, 369, 674–780. (f) Zhao, X.; Pachfule, P.; Thomas, A. Covalent organic frameworks (COFs) for electrochemical applications. *Chem. Soc. Rev.*, **2021**, 50, 6871.

2. (a) Côte, A. P.; Benin, A. I.; Ockwig, N. W.; O'Keeffe, M.; Matzger, A. J.; Yaghi, O. M. Porous, Crystalline, Covalent Organic Frameworks. *Science* **2005**, 310, 1166–1170. (b) Lohse, M. S.; Bein, T. Covalent Organic Frameworks: Structures, Synthesis, and Applications. *Adv. Funct. Mater*. **2018**, 28, 1705553. (c)Haase, F.; V. Lotsch, B. V. Solving the COF trilemma: towards crystalline, stable and functional covalent organic frameworks. *Chem. Soc. Rev*. **2020,** 49, 8469-8500. (d) Peng, L.; Guo, L.; Song, C.; Ghosh, S.; Xu, H.; Wang, L.; Hu, D.; Shi, L.; Zhao, L.; Li, Q.; Sakurai, T.; Yan, T.; Seki, S.; Liu, Y.; Wei, D. Ultra-fast single-crystal polymerization of large-sized covalent organic frameworks. *Nature Communications* **2021**, 12, 5077.
3. (a) Kandambeth, S.; Venkatesh, V.; Shinde, B. D.; Kumari, S.; Halder, A.; Verma, S.; Banerjee, R. Self-templated chemically stable hollow spherical covalent organic framework. *Nature Communications* **2015**, 6, 6786. (b) Sasmal, H. S.; Halder, A.; Kunjattu H, S.; Kaushik Dey, K.; Nadol, A.; Ajithkumar, A. T.; Prachiti Ravindra Bedadur, P. R.; Banerjee, R. Covalent Self-Assembly in Two Dimensions: Connecting Covalent Organic Framework Nanospheres into Crystalline and Porous Thin Films. *J. Am. Chem. Soc*. **2019**, 141, 20371-20379. (b) Nguyen, H. L.; Gropp, C.; Ma, Y.; Zhu, C.; Yaghi, O. M.; 3D Covalent Organic Frameworks Selectively Crystallized through Conformational Design. *J. Am. Chem. Soc*. **2020**, 142, 20335-20339.
4. (a) Fan, H.; Mundstock, A.; Feldhoff, A.; Knebel, A.; Gu, J.; Meng, H.; Caro, J. Covalent Organic Framework-Covalent Organic Framework Bilayer Membranes for Highly Selective Gas Separation. *J. Am. Chem. Soc*. **2018**, 140, 10094-10098. (b) Zhang, W.; Zhang, L.; Zhao, H.; Bin Li, B.; Ma, H. A two-dimensional cationic covalent organic framework membrane for selective molecular sieving. *J. Mater. Chem. A* **2018**, 6, 13331–13339. (c) Wang, H.; Zeng, Z.; Xu, P.; Li, L.; Zeng, G.; Xiao, R.; Tang, Z.; Huang, D.; Tang, L.; Lai, C.; Jiang, D.; Liu, Y.; Yi, H.; Qin, L.; Ye, S.; Ren, X.; Tang, W. Recent progress in covalent organic framework thin films: fabrications, applications and perspectives. *Chem. Soc. Rev*. **2019**, 48, 488-516.
5. (a) Medina, D. D.; Rotter, J. M.; Hu, Y.; Dogru, M.; Werner, V.; Auras, F.; Markiewicz, J. T.; Knochel, P.; Bein T. Room Temperature Synthesis of Covalent-Organic Framework Films through Vapor-Assisted Conversion. *J. Am. Chem. Soc*. **2015**, 137, 1016-1019. (b) Chen, Y.; Cui, H.; Zhang, J.; Zhao, K.; Ding, D.; Guo, J.; Li, L.; Tian, Z.; Tang, Z. Surface growth of highly oriented covalent organic framework thin film with enhanced photoresponse speed. *RSC Adv*. **2015**, 5, 92573–92576. (c) M. Rotter, J. M.; Weinberger, S.; Kampmann, J.; Sick, T.; Shalom, M.; Bein, T.; Medina, D. D. Covalent Organic Framework Films through Electrophoretic Deposition-Creating Efficient Morphologies for Catalysis. *Chem. Mater*. **2019**, 31, 10008-10016.
6. (a) Dey, K.; Pal, M.; Rout, K. C.; Kunjattu H, S.; Das, A.; Mukherjee, R.; Kharul, U. K.; Banerjee, R. Selective Molecular Separation by Interfacially Crystallized CovalentOrganic Framework Thin Films. *J. Am. Chem. Soc*. **2017**, 139, 13083-13091. (b) Sick, T.; Hufnagel, A.G.; Kampmann, J.; Kondofersky, I.; Calik, M.; Rotter, J.M.; Evans, A.; Dӧblinger, M.; Herbert, S.; Peters, K.; Bӧhm, D.; Knochel, P.; Medina, D. D.; Rohlfing, D. F.; Bein, T. Oriented Films of Conjugated 2D Covalent Organic Frameworks as Photocathodes for Water Splitting. *J. Am. Chem. Soc*. **2018**, 140, 2085-2092. (c) Shinde, D. B.; Sheng, G.; Li, X.; Ostwal, M.; Emwas, A. H.; Huang, K. W.; Lai, Z. Crystalline 2D Covalent Organic Framework Membranes for HighFlux Organic Solvent Nanofiltration. *J. Am. Chem. Soc*. **2018**, 140, 14342-14349. (d) Hao, Q.; Juan Li, Z. J.; Lu, C.; Sun, B.; Zhong, Y. W.; Wan, L. J.; Wang, D. Oriented Two-Dimensional Covalent Organic Framework Films for Near-Infrared Electrochromic Application. *J. Am. Chem. Soc*. **2019**, 141, 19831-19838.
7. (a) Zhou, D.; Tan, X.; Wu, H.; Tian, L.; Li, M. Synthesis of C-C Bonded Two-Dimensional Conjugated Covalent Organic Framework Films by Suzuki Polymerization on a Liquid–Liquid Interface. *Angew. Chem. Int. Ed*. **2019**, 58, 1376 –1381. (b) Liu, J.; Han, G.; Zhao, D.; Lu, K.; Gao, J.; Chung, T.S. Self-standing and flexible covalent organic framework (COF) membranes for molecular separation. *Sci. Adv*. **2020**, 6, 41. (c) Sahabudeen, H.; Qi, H.; Ballabio, M.; Položij, M.; Olthof, S.; Shivhare, R.; Jing, Y.; Park, S.; Liu, K.; Zhang, T.; Ma, J.; Rellinghaus, B.; Mannsfeld, S.; Heine, T.; Bonn, M.; Cánovas, E.; Zheng, Z.; Kaiser, U.; Dong, R.; Feng, X. Highly Crystalline and emiconducting Imine-Based Two-DimensionalnPolymers Enabled by Interfacial Synthesis. *Angew. Chem. Int. Ed*. **2020**, 59, 6028 – 6036.
8. (a) Ameloot, R.; Vermoortele, F.; Vanhove, W.; Roeffaers, M. B. J.; Sels, B. F.; De Vos, D. E. Interfacial synthesis of hollow metal–organic framework capsules demonstrating selective permeability. *Nature Chemistry*, **2011**, 3, 382-387. (b) Karan, S.; Jiang, Z.; Livingston, A. G. Sub–10 nm polyamide nanofilms with ultrafast solvent transport for molecular separation. *Science* **2015**, 348 (6241), 1347-1351. (c) Liu, K.; Qi, H.; Dong, R.; Shivhare, R.; Addicoat, M.; Zhang, T.; Sahabudeen, H.; Heine, T.; Mannsfeld, S.; Kaiser, U.; Zheng, Z.; Xinliang Feng, X. On-water surface synthesis of crystalline, few-layer two-dimensional polymers assisted by surfactant monolayers. *Nature Chemistry* **2019**, 11, 994-1000.
9. (a) Feldblyum, J. I.; McCreery, C. H.; Andrews, S. C.; Kurosawa, T.; Santos, E. J. G.; Duong, V.; Fang, L.; Ayzner, A. L.; Bao, Z. Few-layer, large-area, 2D covalent organic framework semiconductor thin films. *Chem. Commun*. **2015**, 51, 13894-13897.
10. (a) Zhong, Y.; Cheng, B.; Park, C.; Ray, A.; Brown, S.; Mujid, F.; Lee, J. U.; Zhou, H.; Suh, J.; Lee, K. H.; Mannix, A. J.; Kang, K.; Sibener, S. J.; Muller, D. A.; Park, J. Wafer-scale synthesis of monolayer two-dimensional porphyrin polymers for hybrid superlattices. *Science* **2019**, 366, 1379–1384.
11. (a) Cai, S. L.; Zhang, Y. B.; Pun, A. B.; He, B.; Yang, J.; Toma, F. M.; Sharp, I. D.; Yaghi, O. M.; Fan, J.; Zheng, S. R.; Zhang, W. G.; Liu, Y. Tunable electrical conductivity in oriented thin films of tetrathiafulvalene-based covalent organic framework. *Chem. Sci*. **2014**, 5, 4693–4700. (b) Evans, A. M.; Giri, A.; Sangwan, V. K.; Xun, S.; Matthew Bartnof, M.; Torres-Castanedo, C. G.; Balch, H. B.; Rahn, M. S.; Bradshaw, N. P.; Vitaku, E.; Burke, D. W.; Li, H.; Michael J. Bedzyk, M. J.; Wang, F.; Brédas, J. L.; Malen, J. A.; McGaughey, A. J. H.; Hersam, M. C.; Dichtel, W. R.; Hopkins, P. E. Thermally conductive ultra-low-k dielectric layers based on two-dimensional covalent organic frameworks. *Nature Materials* **2021**, 20, 1142-1148.
12. (a) Dey, K.; Mohata, S.; Banerjee, R. Covalent Organic Frameworks and Supramolecular Nano-Synthesis. *ACS Nano* **2021**, 15, 8, 12723–12740.

13. (a) Halder, A.; Karak, S.; Addicoat, M.; Bera, S.; Chakraborty, A.; Kunjattu, S. H.; Pachfule, P.; Heine, T.; Banerjee, R. Ultra-stable Imine-based Covalent Organic Frameworks for Sulfuric acid Recovery: An Effect of Interlayer Hydrogen Bonding. *Angew. Chem. Int. Ed.* **2018**, 57, 5797.
14. (a) Barker, I. K.; Fawcett, V.; Long, D.A. Solvent Dependence of the Resonance Raman Spectra of Azobenzene, 4-Aminoazobenzene, 4-Methylaminobenzene and 4-Dimethylaminoazobenzene. *Journal of Raman Spectroscopy* **1987**, 18, 71-75. (b) Stuart, C. M.; Frontiera, R. R.; Mathies, R. A. Excited-State Structure and Dynamics of cis- and trans-Azobenzene from Resonance Raman Intensity Analysis. *J. Phys. Chem. A* **2007**, 111, 12072-12080. (c) Tsuboi, M.; Benevides, J. M.; Thomas Jr, G. J. The Complex of Ethidium Bromide with Genomic DNA: Structure Analysis by Polarized Raman Spectroscopy. *Biophysical Journal* **2007**, 92, 928–934.
15. (a) Desiraju, G.R. Supramolecular Synthons in Crystal Engineering-A New Organic Synthesis. *Angew. Chem. Int. Ed.* **1995**, 31, 2311-2321. (b) Desiraju, G. R.; Steiner, T. The Weak Hydrogen Bond: In Structural Chemistry and Biology; Oxford University Press: Oxford and New York, **2001**.
16. (a) Huang, W.; Jiang, Y.; Li, X.; Li, X.; Wang, J.; Wu, Q.; Liu, X. Solvothermal Synthesis of Microporous, Crystalline Covalent Organic Framework Nanofibers and Their Colorimetric Nanohybrid Structures. *ACS Appl. Mater. Interfaces* **2013**, 5, 8845–8849. (b) Sasmal, H. S.; Bag, S.; Chandra, B.; Majumder, P.; Kuiry, H.; Karak, S.; Gupta, S. S.; Banerjee, R. Heterogeneous C-H Functionalization in Water via Porous Covalent Organic Framework Nano Films: A Case of Catalytic Sphere Transmutation. *J. Am. Chem. Soc.* **2021**, 143, 8426.
17. (a) Li, T.; Zhang, W. D.; Liu, Y.; Li, Y.; Cheng, C.; Zhu, H.; Yan, X.; Li, Z.; Gu, Z. G. A two-dimensional semiconducting covalent organic framework with nickel (II) coordination for high capacitive performance. *J. Mater. Chem. A* **2019**, 7, 19676–19681. (b) Mahringer, A.; Jakowetz, A. C.; Rotter, J. M.; Bohn, B. J.; Stolarczyk, J. K.; Feldmann, J.; Bein, T.; Medina, D. D. Oriented Thin Films of Electroactive Triphenylene Catecholate-Based TwoDimensional Metal-Organic Frameworks. *ACS Nano* **2019**, 13, 6711-6719. (c) Souto, M.; Perepichka, D. F. Electrically conductive covalent organic frameworks: bridging the fields of organic metals and 2D materials. *J. Mater. Chem. C* **2021**, 9, 10668-10676.
18. The film thickness of 120 ± 20 nm was maintained for all the residual films, direct synthesis, and solvothermal synthesis. We underwent difficulty transferring a macroscopic defect-free, large area thinner COF film onto a substrate. So, we synthesized a marginally thick film (170 ± 10 nm) for conductivity measurement of interfacial thin films. For the spin coating method also, we faced difficulty growing a continuous thin film on the substrate, which compelled us to synthesize a thick film of thickness 235 ± 25 nm.
19. (a) Sun, L.; Campbell, M. G.; Dincaˇ, M. Electrically Conductive Porous Metal–Organic Frameworks. *Angew. Chem. Int. Ed.* **2016**, 55, 3566 – 3579.
20. (a) Aubrey, M. L.; Wiers, B. M.; Andrews, S. C.; Sakurai, T.; Reyes-Lillo, S. E.; Hamed, S. M.; Yu, C-J.; Darago, L. E.; Mason, J. A.; Baeg, J-O.; Grandjean, F.; Long, G. J.; Seki, S.; Neaton, J. B.; Yang, P.; Long, J. R. Electron delocalization and charge mobility as a function of reduction in a metal–organic framework. *Nat. Mater.* **2018**, 17, 625–632.

Table of Contents